All-inkjet printed gold microelectrode arrays for extracellular recording of action potentials

Bernd Bachmann[1,2], Nouran Y Adly[1], Jan Schnitker[1], Alexey Yakushenko[1], Philipp Rinklin[2], Andreas Offenhäusser[1] and Bernhard Wolfrum[*,1,2]

[1] Peter Grünberg Institute (PGI-8, Bioelectronics), Forschungszentrum Jülich GmbH, 52425 Jülich, Germany

[2] Neuroelectronics, MSB, Department of Electrical and Computer Engineering, Technical University of Munich (TUM) & BCCN Munich, 85748 Garching, Germany

E-mail: bernhard.wolfrum@tum.de

Abstract. Inkjet printing is an attractive method for cost-effective additive manufacturing of electronic devices. Especially for applications where disposable sensor systems are of interest, it is a promising tool since it enables the production of low-cost and flexible devices. In this work, we report the fabrication of a disposable microelectrode array using solely inkjet-printing technology. We apply the printed device for extracellular recording of action potentials from cardiomyocyte-like HL-1 cells. The microelectrode arrays were fabricated with two different functional inks, a self-made gold ink to print conductive feedlines and electrodes and a polymer-based ink to add a dielectric layer for insulation of the feedlines. We printed different microelectrode array designs of up to 64 electrodes with a minimum lateral spacing of 200 µm and a minimum electrode diameter of ~31 µm. As a proof-of-concept, extracellular recordings of action potentials from HL-1 cells were performed using the all-printed devices. Furthermore, we stimulated the cells during the recordings with noradrenaline, which led to an increase in the recorded beating frequency of the cells. The results demonstrate the feasibility of inkjet-printing gold microelectrode arrays for cell-based bioelectronics.

Keywords: inkjet printing, gold ink, microelectrode array, bioelectronics, extracellular recording of action potentials

* Corresponding author: bernhard.wolfrum@tum.de

1. Introduction

The extracellular recording of neuronal and muscle cells using electrode arrays is a powerful method to investigate and understand bioelectronic systems. While large electrodes are usually applied for bioelectronics systems such as electrocardiography or electromyography, microelectrode arrays (MEAs) can be used to study effects on the single-cell or cell-network level. This includes, for example, the examination of pharmaceutical or toxicological effects of drugs and chemicals on neuronal networks [1–5], studies on neurotransmitter release [6,7], or the investigation of the communication pathway of individual neurons [8,9]. MEAs also allow to stimulate nervous or muscle tissue [10–13], and can be used as electrochemical sensors to detect, for instance, low concentrations of silver nanoparticles [14]. Over the past decades, a lot of effort has been directed towards improving the interface between MEAs and cells. Recent approaches for MEA optimization range from 3D-architectures and surface modifications to improve the cell-chip coupling [15–20] to CMOS-based MEAs in order to increase the spatial resolution of recording electrode arrays [8,9]. For example, Müller *et al*. fabricated a MEA that comprises 26400 electrodes, being capable of recording 1024 channels in parallel [9]. Recent research focused on the development of soft and flexible microelectrode arrays [21–27] including injectable electronic meshes for *in vivo* studies to access information from, e.g., the cerebral cortex [28].

Clean-room-fabricated MEAs have been demonstrated to be powerful tools for extracellular recording of action potentials. However, major disadvantages of clean-room technology are the high cost and often time-consuming and complex fabrication processes. For example, a limiting factor in optical lithography is the requirement of masks for each lithographic step. As a consequence, changes in the design are difficult to implement, rendering adaptive fabrication and prototyping time-consuming and expensive. Moreover, fabricating MEAs on flexible low-cost substrates is often not compatible with standard clean-room processing, which is inconvenient for the development of disposable sensor systems.

Considering these disadvantages, printing methods have moved into the focus as an alternative promising fabrication method. In particular, inkjet printing allows the simple, cost-effective and contactless, additive manufacturing of electronic devices [29]. The manufacturer can easily change the desired design. The possibility of using a broad range of materials as inks enables printing a variety of devices. Examples for materials include conductive polymers, nanotubes, semiconducting materials, dielectric inks, proteins or even living cells [30–35]. These advantages allow printing a wide range of sensor types such mechanical sensors or biosensors [36–39]. A very recent example was reported by Vourinen *et al.*, who used a graphene/PEDOT:PSS ink to fabricate an inkjet-printed skin-conformable temperature sensor [40]. These examples as well as the simple, fast, and cheap fabrication process make inkjet printing a promising tool for the fabrication of disposable microelectrode arrays.

Several groups have already reported inkjet-printed gold electrodes, sensors, and printed MEAs [41–46]. However, previous examples either suffer from a relatively low resolution or involve additional clean-room fabrication steps. Roberts *et al.* fabricated inkjet-printed PEDOT:PSS conductive-polymer electrode arrays with 28 4x4 mm² electrodes, which they used for *in vivo* electromyography and electrocardiography measurements [47]. Khan *et al.* recently presented an inkjet-printed microelectrode array fabricated using a gold nanoparticle ink [48]. In their work, inkjet-printed gold lines were covered by a spin-coated polymer. Subsequent etching steps yielded 31 flexible free-standing electrode flaps with a minimum feature size of 64 µm and an electrode pitch of 2-7 mm. The same groups developed a MEA comprising 55 electrodes with a diameter of 500 µm and an electrode spacing of 2.54 mm, which was applied for impedance measurements to detect pressure ulcers in a rat model *in vivo* [49].

In this report, we present the fabrication of low-temperature sintered gold MEAs for cell recordings using solely inkjet technology. In figure 1, the printing process of the MEA and the cell recording are illustrated. Two different MEA designs were printed using a self-made gold ink. The first layout contains 28 electrodes with an electrode pitch of 400 µm. The second layout exhibits an improved resolution of the MEA containing 64 electrodes with an electrode pitch of 200 µm.

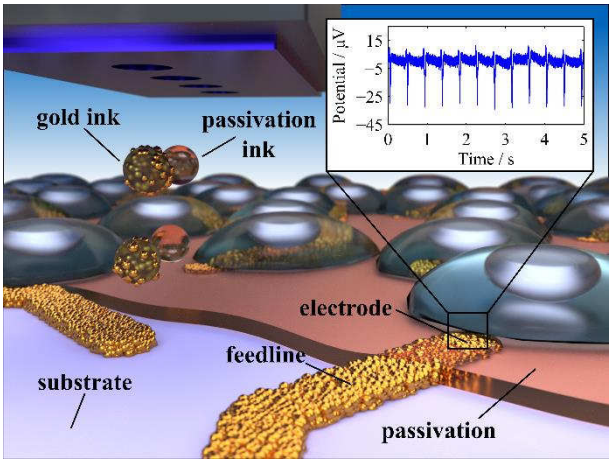

Figure 1. The schematic combines a description of the overall printing process of the MEA (left) with an illustration of the recording of cells with a printed microelectrode (right). On the upper left side, drops of the gold and passivation ink are ejected from the printhead and are subsequently deposited on the substrate to form conductive feedines (gold) and the insulating layer (red). The printed microelectrodes are used to perform extracellular recordings of action potentials (upper right) from the overlaying cells (gray).

The MEAs were fabricated in two main steps. First, the conductive feedlines were printed on a thin polymeric substrate using a gold nanoparticle-based ink. Subsequently, an insulating layer was printed using a dielectric polymer-based ink. Gold was chosen for the electrode material since it provides good conductivity, chemical stability, and biocompatibility. The latter is essential for performing extracellular recordings in an electrolytic environment.

As a proof-of-concept, spontaneous, as well as chemically stimulated, action potentials of cardiomyocyte-like HL-1 cells were recorded using the printed MEA. With this, we demonstrate the feasibility of inkjet-printed microelectrodes for bioelectronic investigations at the cellular level.

2. Experimental section

Printing methods and ink development

All structures presented herein were fabricated using a drop-on-demand inkjet printer (UniJet™ OJ300) with a piezo-driven printhead. The printer features a positioning accuracy of ± 5 µm and a position repeatability of ± 1 µm. For the conductive feedlines, a self-made gold nanoparticle-based ink was developed. The gold nanoparticles were synthesized according to the Brust-Schiffrin method (see supplementary information).

For the dielectric layer, a polyimide-based (PI) ink was purchased (PIN 6400-001, Chisso Coorporation). Both inks were loaded into a 10 pL cartridge (DMC-11610, Dimatix™) or a 1 pL cartridge (DMC-11601, Dimatix™) via a hydrophobic PTFE filter (0.1 µm pore size). Jetting behaviour was observed using the printer's software tools.

Printing of test patterns

Prior to printing the MEAs, substrate-ink interactions were evaluated by printing test patterns on two substrates: (1) flexible polyimide-based (PI) Kapton® (DuPont™) and (2) polyethylene naphtalate-based substrate Optfine® PQA1M (DuPont Teijin Films). The test patterns were printed using both inks. The structures were optically analyzed using differential interference contrast (DIC) microscopy. The dimensions were analyzed using the image analysis tool "ImageJ". Additional analysis of the morphology of the printed gold layers was carried out using scanning electron microscopy (SEM).

Printing microelectrode arrays

Two layouts of MEAs were printed for evaluation. The first one was a low-resolution layout with an array comprising 28 electrodes within an area of 25.4 × 25.4 mm². This layout was printed on a polyimide-based substrate (125 µm thickness, Kapton®, DuPont™). First, the feedlines were printed with one layer of gold and a drop spacing of 36.7 µm. Subsequently, the gold layer was thermally sintered by heating the Kapton® substrate to 200 °C at a rate of 3.3 °C min^{-1} and tempering at this temperature for 1 h. In a second printing step, the feedlines were passivated with the PI at a drop spacing of 36.7 µm. Here, up to three layers were printed subsequently one after the other to sufficiently cover the conducting feedlines of the MEA. Printing a single layer for a MEA of 25.4 x 25.4 mm² lasts approx.. 30 min providing sufficient drying time in between successive layers. Above the end of the feedlines, an opening with an approximate diameter of 180 µm was left for the electroactive area. Printing a single layer for a MEA of 25.4 x 25.4 mm² lasts approx. 30 min providing sufficient drying time in between successive layers. After printing, the insulating polyimide was cross-linked at 200 °C for 1 h. The second layout was based on a typical clean-room fabricated MEA with a higher electrode density (64 electrodes, 200 µm electrode spacing [6]) within an area of 10.6 × 10.6 mm². Due to the increased resolution of the layout, devices were printed on a PQA1M substrate. The conductive lines were deposited with one layer of gold and a drop spacing of 20 µm. The gold layer was heated up to 125 °C and sintered for 60 min at this temperature. Prior to depositing the insulating layer, the sample was activated using oxygen plasma. The operational parameters were a pressure of 0.8 mbar and a power of 120 W for 30 s (Zepto, Diener Electronics). Three layers of PI ink were printed at a drop spacing of 25 µm to 30 µm until a continuous insulating film was obtained. Table S1 in the supplementary information provides detailed information on the fabrication process and the printing parameters for both layouts.

Electrical and electrochemical characterization

Four-point resistance measurements were performed on gold structures printed on a PQA1M substrate sintered at different temperatures ranging from 107 °C to 201 °C. In an additional experiment, the resistance of 21.7 mm long tracks printed on Kapton® was measured. The lines were printed with one, two, and three layers using a drop spacing of 36.7 µm. Two different line widths (1 pixel and 3 pixels) were investigated. To calculate the specific resistivity, the thickness of the sintered lines was obtained by profilometric measurements.

In order to determine basic electrode characteristics, printed gold structures were electrochemically analyzed in terms of their specific capacitance by means of impedance spectroscopy using a multiple channel potentiostat (VSP-300, Bio-Logic Science Instruments, France) controlled by the software "EC-Lab v10.19". To determine the specific capacitance, a 10 × 10 mm² square of gold was printed on the PI substrate. A glass ring with an inner diameter of 7 mm was glued onto the gold surface with polydimethylsiloxane (Sylgard 184, Dow Corning, Midland, USA). Phosphate buffered saline (PBS) was pipetted into the glass ring covering an area of 0.385 cm². To determine the specific capacitance, the impedance was measured in a three-electrode configuration. The working electrode was connected to the printed gold and the impedance was measured against a Ag/AgCl quasi-reference electrode dipped in the PBS solution. The impedance was recorded from 100 kHz to 10 Hz with a sinusoidal excitation potential of 10 mV. The specific capacitance was then extracted by fitting the impedance data against a Randles circuit without a Warburg impedance [50].

For the characterization of the MEAs, impedance measurements were performed as stated above, but with a combined reference and counter-electrode. To this end, the microelectrode arrays were mounted onto a substrate carrier connected to a socket via the contact pads, which allowed addressing each of the electrodes individually. To analyze the electrochemical performance, the capacitance of each electrode was determined. If the capacitance of the electrodes of the second layout was in between 20 pF and 400 pF, the electrodes were considered suitable for further measurements.

Recording of action potentials of cardiomyocytes

Before plating cells on the microelectrode arrays (layout 1), the MEAs were rinsed with deionized water and sterilized with UV light for 30 min under a sterile bench. A protein coating for the adhesion of HL-1 cells was performed by incubating the sensor array using 50 µL of a solution of 0.2% (v/v) gelatin together with 5 µg mL^{-1} fibronectin in bi-distilled water for one hour. Afterwards, the protein solution was removed and the MEA was rinsed with PBS. Cardiomyocyte-like cells (HL-1) [51] were cultured on the printed MEAs following the protocol of [17] until they reached a confluent layer after several days, in this case after 3-4 days *in vitro* (DIV) [12]. Electrical recordings were performed using an in-house built recording and amplifying system ('BioMAS') customized for recording and stimulation of cells via 64 electrodes. The encapsulated MEA was connected to the head stage socket of the amplifier system, which is able to record 64 electrodes in parallel with a sampling rate of 10 kHz. The measurement system was grounded and shielded by a Faraday cage. The recording electrode voltages were measured against a Ag/AgCl quasi-reference electrode and amplified by a factor of ten in the headstage and further amplified by a factor of 100 in the main amp. The measurements were performed AC coupled and had an effective bandwidth of 1 Hz to 3 kHz. The electrical measurements were performed for two microelectrode arrays at DIV 3 and 4. First, spontaneous *action potentials* were measured. To test whether an externally induced stimulus can be recorded, the cells were chemically stimulated. We subsequently applied 20 µl and 40 µl of 1 mM noradrenaline solution to the cell culture medium (1 ml). The measurements were performed for a time period of approximately 1 min. After the application, the beating of the cells was stopped by adding 200 µl of 1 M of sodium dodecyl sulphate (SDS). The recordings were performed with an AC coupling at a cut-off frequency 1 Hz. The signal was imported into Matlab and a low order polynomial fit was subtracted from the data in order to remove baseline fluctuations in the lower frequency regime above the cut-off frequency. Data analysis of the signal was performed with a custom Matlab code to determine firing rate and peak-to-peak amplitudes of the recorded spikes. The signal-to-noise ratio (SNR) was obtained by relating the average peak-to-peak amplitude of the action potential traces to the root-mean-square (RMS) noise of the traces.

3. Results and discussion

Characterization of inkjet-printed patterns

Prior to printing, the drop formation of both inks, the gold ink and the polymer ink was characterized. In figure 2, stroboscopic image series of an ejected drop of the gold nanoparticle-based (a) and polyimide (PI)-based (b) ink are shown. For both inks, stable drops could be generated. Whereas the ejection of the gold ink exhibit small single droplets, the ejection of the PI ink results in small droplets that are followed by long ligaments, which increase the overall drop volume.

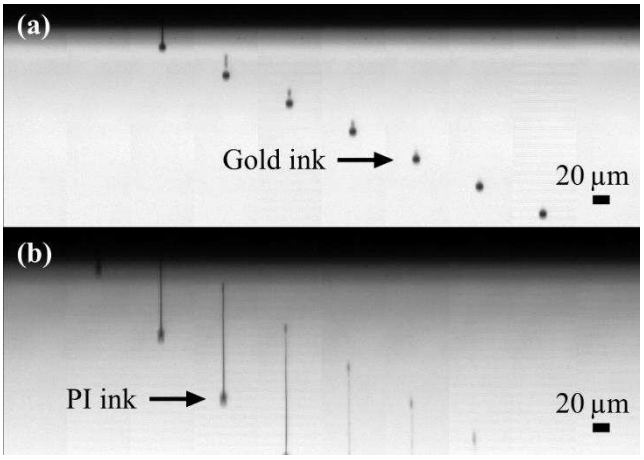

Figure 2. Stroboscopic image series of an ejected drop of the gold nanoparticle-based (a) and polyimide (PI)-based (b) ink.

The resolution of printed structures mainly depends on the amount of deposited material as well as on the substrate-ink interactions. In particular, the choice of substrate can significantly alter the resolution of printed structures. Test patterns were printed on the two substrates PI (Kapton®) and PQA1M, which differ in the surface texture and surface energy (37.5 mN m^{-1} and 31.5 mN m^{-1}, respectively). Figure 3 shows images of the wetting behaviour and structures printed on Kapton® (left column) and PQA1M (right column). As it can be seen from figure 3(a), the contact angle of the gold ink on Kapton® is significantly lower than the contact angle on PQA1M (figure 3(b)) and no exact values could be measured due to complete wetting of the ink on the substrate. Using a 10 pl cartridge, the width of a printed single-droplet line on Kapton® was about 90 µm, which was significantly higher than the width of a line printed on PQA1M (~40 µm, compare figure 3(c) and (d)). Using a 1 pl cartridge the width of a single droplet on PQA1M could be further reduced to approximately 27 µm. Whereas the larger feature size of gold structures on Kapton® enable printing MEAs with the low-resolution design (layout 1), the small structures on PQA1M facilitate printing of small-scaled MEAs with a higher electrode density (layout 2). This significant reduction of the pattern's dimensions on PQA1M in contrast to PI is assigned to the lower surface energy as well as to the more planar surface and a better pinning of the ink on the PQA1M substrate. Since only small amounts of ink were prepared for each printing session, batch-to-batch variations may induce slight differences in the printed structures.

After printing conductive tracks, the feedlines of the MEA have to be insulated to prevent leakage currents during cell measurements. Figures 3(e) and (f) show images of test squares printed on Kapton® (1 layer) and PQA1M (3 layers), respectively. In both cases the squares exhibited a smooth outline. However, a small elevation could be seen at the rim of the squares, which increased for a decreased drop spacing and for a higher number of printed layers. We attribute this to the so-called coffee-ring effect. This effect originates from a flow driven by surface tension from the center to the edge upon evaporation of the ink solvent. The nature of the coffee-ring effect has been extensively described elsewhere [52,53]. The coffee-ring effect is not assumed to significantly affect the MEA performance as long as the central parts of the insulation layer are fully covered with dielectric material.

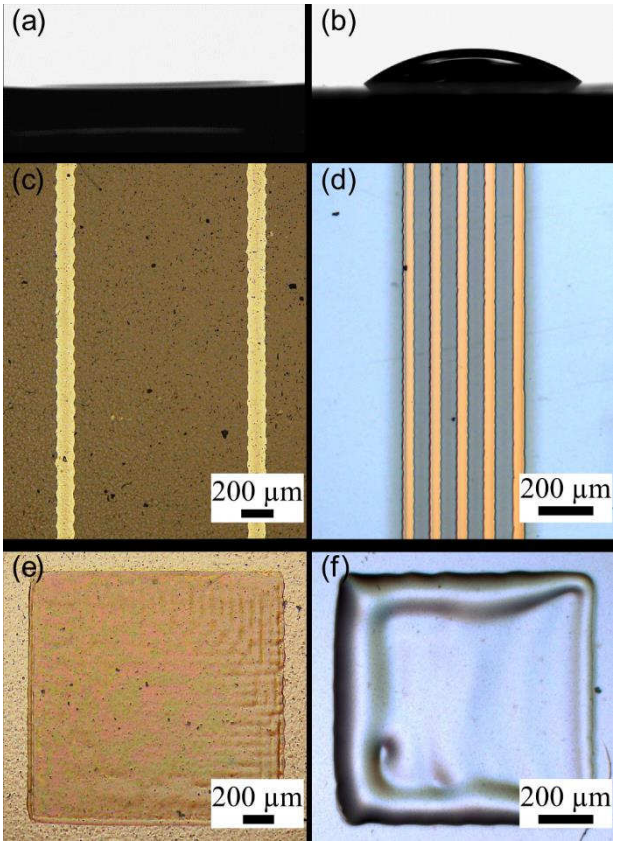

Figure 3. Comparison of the substrate-ink-interactions for the Kapton® substrate (left column) with a high surface energy and for the PQA1M substrate (right column) with a low surface energy. In (a) and (b) the contact angle is shown for both substrates.Corresponding gold line patterns are shown in (c) and (d). Printed polyimide test structures are presented for Kapton® (1 layer) and PQA1M (3 layers) in (e) and (f), respectively

Electrical and electrochemical characterization of the inks

The printed gold was electrically and electrochemically characterized. Here, the benefits of using gold as an electrode material become obvious, as gold is chemically inert and provides good electrochemical and conductive properties. These properties are essential for electrochemical and especially for bioelectronic investigations such as the recording of cardiomyocyte or neuronal action potentials. Moreover, gold can be used in the form of nanoparticles as an ink. This is beneficial since the sintering temperature of conductive particles reduces drastically with decreasing particle size [54]. This allows to print and sinter the gold film on thin flexible polymer substrates that usually exhibit a low melting temperature and a low heat shrinkage. The PQA1M substrate used in our studies has a glass transition temperature of as low as 121 °C and a melting point of as low as 269 °C. Despite this low thermal stability, we were able to successfully print and sinter gold structures on this substrate as described below.

Hence, after characterizing the basic printing behavior as described above, the electrical behavior of the custom low temperature-sintering gold-nanoparticle ink was evaluated in terms of the resistivity. In figure 4(a), the sheet resistance of printed gold lines on a PQA1M substrate is plotted as a function of the sintering temperature ranging from 107 °C to 201 °C. As can be seen, the samples already exhibited acceptable conducting properties at low sintering temperatures. Increasing the sintering temperature reduced the resistance significantly from 138 ± 17 Ω $\square^{-1}$ at 107 °C down to approx. 75 ± 18 Ω $\square^{-1}$ at 201 °C. This demonstrates the polymer-compatible low sintering temperature of the gold ink.

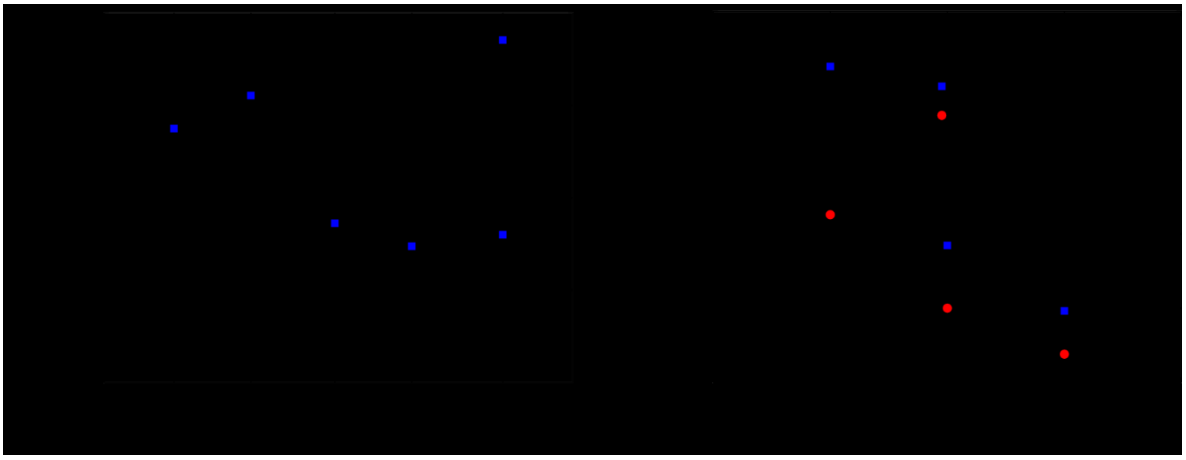

Figure 4. (a) Sheet resistance of printed gold lines as a function of different sintering temperatures (n = 3). The temperature was increased with 3.3 °C/min up to the indicated sintering temperature. (b) Sheet resistance as a function of the number of printed layers for a line width of one and three pixels with a drop spacing of 36 µm.

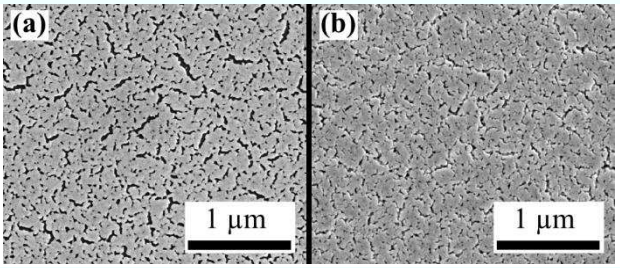

Figure 5. SEM images of the sintered gold samples on Kapton® show that increasing the number of printed layers from one (a) to three (b) leads to a denser gold film.

However, due to the low heat stability, large sheets (approx. 10 x 15 cm^2) of the PQA1M substrate started deforming and became rigid, when sintered at a temperature of 200 °C. Although the small area on the spreadsheet occupied by the MEA was negligibly affected by the heat instability issues, further gold lines for the resistance experiments were printed on Kapton® substrate since it exhibits a better heat stability.

In figure 4(b) the sheet resistance of electrode feedlines (one and three pixels in width) for different number of printed layers are shown. As expected, the sheet resistance can be significantly reduced by adding successively printed gold layers. This is in accordance with the assumption that printing several layers leads to more gold nanoparticles being deposited per area, which in turn results in a denser and thicker gold film. This can be validated by the corresponding SEM images in figure 5. Here, the porous structure (the dark area contributes to the pores in the upper layer of the conductive material) of the sintered gold can be seen for one (a) and three (b) printed layers. Analysis of the two images revealed a coverage of 88% for a single layer and 95% for three layers. The gold porosity is mainly affected by the amount of gold deposited on the substrate. Whereas different surface energies of the substrates might influence the height and the diameter of a single drop, the amount of gold can be appropriately adjusted by the drop spacing. In case of the printed lines (length of ~22 mm), the sheet resistance is in the range of 0.69 $\Omega\ \square^{-1}$ to 2.63 $\Omega\ \square^{-1}$. The thickness of the printed lines for one, two and three printed gold layers was 112 ± 10 nm, 313 ± 32 nm and 777 ± 25 nm, respectively. The thickness was used to calculate the

specific resistivity. In total, a resistivity of (18-76) × 10^{-8} Ω m was obtained, which is in accordance with values obtained by other studies [55–58].

During the cell recording, the gold microelectrode is exposed to an electrolytic environment. The impedance formed by the electrode/electrolyte interface is a dominating factor in the quality of electrical or electrochemical measurements. Hence, the specific capacitance of the printed gold was measured by impedance spectroscopy. Here, the specific capacitance was (45 ± 21) × 10^{-2} F m^{-2}. This is comparable to values obtained for bulk gold, which are typically in the range of /10-100) × 10^{-2} F m^{-2} [59]. Thus, it is assumed that the printed gold shows appropriate properties for electrochemical measurements. The deviation to bulk gold might be explained by the porous structure of the sintered gold (compare figure 5), and the associated larger area of the effective gold surface.

Development and characterization of the inkjet-printed microelectrode array

We subsequently printed the conductive gold ink and insulating PI ink to fabricate two types of microelectrode arrays. The lower-resolution layout was printed on a Kapton substrate for the demonstration of electrophysiological recordings. The second layout printed on PQA1M exhibits a higher electrode density with a better resolution of printed structures. This layout was used to demonstrate that devices comparable to conventional clean-room fabricated MEAs can be produced using solely inkjet printing technology. The overall success rate of printing microelectrodes obtained for three chips for layout 1 and layout 2 was 94% (n = 84 electrodes) and 72% (n = 192), respectively. In figure 6(a) and (b), the first layout with 28 feedlines was printed on the Kapton® foil. The final MEA mounted to a substrate carrier can be seen in figure 6(a). Figure 6(b) shows a microscopic image of the central electrode area.

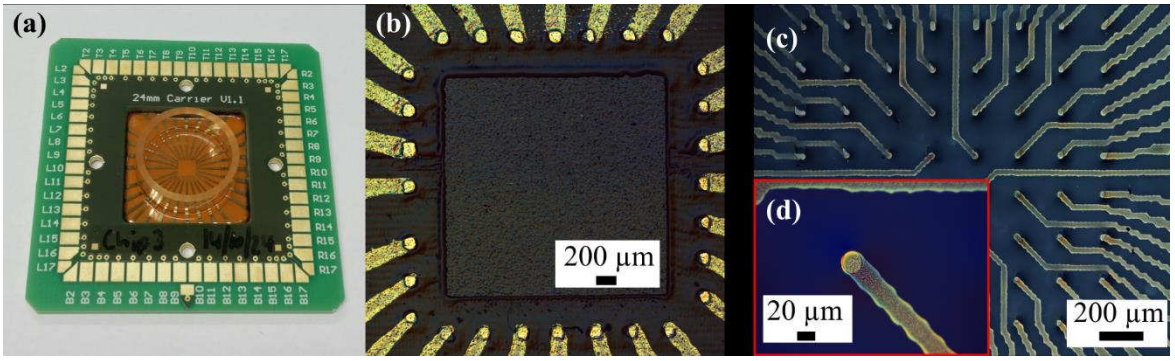

Figure 6. (a) Printed MEA on the Kapton® substrate (layout 1), which is comprised of 28 gold electrodes. The MEA is mounted onto a substrate carrier to connect it to the amplifying measurement system. (b) Microscopic image of the central part of the MEA on the Kapton® substrate (layout 1). The electrode pitch is 400 µm. (c) Printed MEA (layout 2) with 64 microelectrodes with an electrode pitch of 200 µm. (d) Close-up of a single electrode.

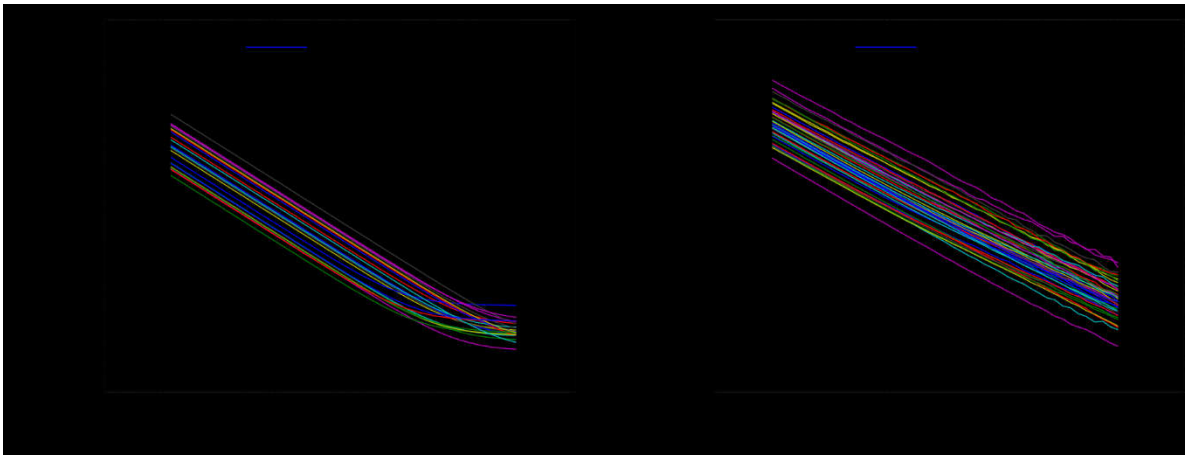

Figure 7. Impedance spectra of printed microelectrodes using the low-resolution layout (a) and the high-resolution layout (b). All recordings were obtained from the same chip. Data from different chips are shown in the figure S1 in the supplementary information.

Optical measurements revealed an electrode area of $(8.4 \pm 2.2) \times 10^{-9}$ m^2 (n = 22). Assuming a circular opening, this corresponds to an electrode diameter of 103 ± 27 µm. The electrode pitch is approximately 400 µm, which is a factor of 2 to 4 larger than the pitch typically seen in conventional MEAs for *in vitro* cell recordings [60]. Nevertheless, both, the pitch and the size of the electrodes could be reduced by optimizing the printing parameters as described above. Figure 6(c) shows the second layout with a printed array of 64 microelectrodes with a pitch of 200 µm and an electrode diameter of (31 ± 7) µm (n = 102). To fabricate these MEAs, PQA1M was used as a substrate due to its low surface energy and printing was performed with a 1 pL cartridge to obtain smaller drop diameters. However, the electrode openings exhibited deviations in the dimensions and shape, which is attributed to different surface chemistry of the printed gold and the substrate and an associated local uncontrollable flow of ink. In figure 6(d) an example of an individual microelectrode is shown. After printing, the impedances of individual microelectrodes were investigated. Figure 7(a) shows the fitted impedance spectra of 22 microelectrodes of a single chip (MEA layout 1) that have been used for cell measurements. For the remaining six electrodes no connection was measured, which might have been caused by broken contacts at the interface of the bond pad and substrate carrier. The impedance spectra of the microelectrodes exhibited a plateau at high frequencies, which was caused by the electrolyte resistance. At low frequencies the capacitive impedance of the microelectrodes dominates. Extracting the double layer capacitance using a simple Randles circuit from the fitted data resulted in a value of (8.1 ± 4.3) nF (n = 22). The corresponding specific capacitance of the gold electrodes was $(97 \pm 57) \times 10^{-2}$ F m^{-2}, which is near the upper limit of the expected range for macroscopic printed gold films rendering them suitable to measure low potentials during cell investigations [12,59,61]. The fitted charge transfer resistance and electrolyte resistance for all fits were in the range of $(1.18 \pm 0.72) \times 10^8$ Ω and (6.4 ± 2.4) kΩ, respectively Figure 7(b) shows the impedance of the high-resolution electrodes from layout 2. As expected, due to the smaller electrode size, the impedance is significantly higher compared to the larger electrodes of layout 1. We obtained a capacitance of (308 ± 230) pF (n = 115), corresponding to a specific capacitance of $(24 \pm 20) \times 10^{-2}$ F m^{-2}. The variation in the impedance spectra may be partially caused by a variation in the active electrode area, which scales inversely with the double layer capacitance at the electrode/electrolyte interface. While we observe a rather large variation between individual electrodes, the average impedance comparing different microelectrode is rather constant (see figure S1 in the supplementary information). The device properties of the two layouts are summarized in the table S1 (see supplementary information).

Extracellular voltage recordings

For the extracellular detection of action potentials, a confluent monolayer of cardiomyocyte-like HL-1 cells was cultured on the printed MEAs (layout 1). The cells showed spontaneous beating behavior indicating cell viability. Action potentials were recorded after 3 to 4 days *in vitro* and exemplary traces are shown in figure 8(a). The action potentials occurred periodically at a frequency of 0.5 Hz, which is in the typical physiological range of 0.1 Hz to 2 Hz. The peak-to-peak (P2P) amplitude of the signals recorded on different electrodes varied strongly between 27 µV and 49 µV resulting in an average amplitude of $P2P_{mean}$ = (36 ± 7) µV (n=11). To evaluate the noise of the recorded signal, the root-mean-square (RMS) value was determined for the recording microelectrodes. The averaged RMS value was RMS = (2.1 ± 0.4) µV, indicating a low noise level. The average signal-to-noise value is SNR = 17. The signal amplitudes are somewhat lower compared to recordings obtained with clean-room fabricated gold MEAs, which also exhibit significant variation but typically lie in the range of several 100 µV or mV [15].

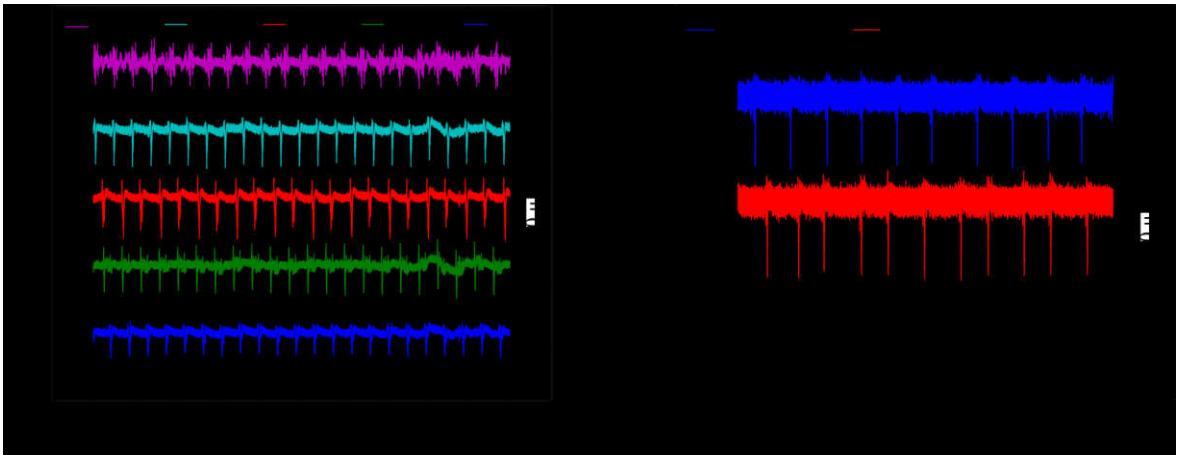

Figure 8. (a) Five traces of action potentials of cardiomyocyte-like HL-1 cells recorded by five printed microelectrodes of layout 1. (b) The action potential was stimulated chemically by noradrenaline. The expected increase in the beating frequency of the HL-1 cells could be recorded by the printed MEA.

The variations in the signals' amplitudes can have several reasons. Heterogeneity of the cell layer and a possible change in the cell-electrode coupling, depending on the cell-substrate interactions, will have a large influence on the signal amplitude. Furthermore, the particular cell passage as well as partial coverage of the sensors could lead to a variation in the recorded signal quality. Additionally, the variations of the electrode area and corresponding changes in the impedance will influence the noise level of the recordings.

In addition to the recording of spontaneous activity, the samples were stimulated chemically by adding the neurotransmitter noradrenaline. Adding noradrenaline increases the beating frequency of the cells. In our experiment, we were able to observe this effect as depicted in figure 8(b). The plots show recordings after addition of 0, 20, and 40 µL of noradrenaline (top to bottom). As can be seen, the spike rate of action potentials increases as a response to the added neurotransmitter. In this particular recording, the spontaneous frequency of 0.33 Hz changed to 0.38 Hz and 0.58 Hz after adding 20 and 40 µL of noradrenaline solution, respectively. In total, this demonstrates that the all-printed MEAs can be used for bioelectronic investigations, e.g., as disposable devices for testing drug effects.

In the future, we envision that further refinements of the printing process may enhance the resolution and density of active sensor array devices. Furthermore, it might be possible to also apply printed microelectrodes for stimulation of cells. To this end, investigations concerning the stability of the printed electrode layer during prolonged stimulation should be investigated.

4. Conclusion

The aim of this work was to fabricate a disposable gold microelectrode array (MEA) for extracellular recordings from cells using solely inkjet printing technology. The printed MEAs were fabricated in two steps. First, a custom gold ink was used to print conductive tracks on flexible polymer-based substrates. In a post-processing step, the printed gold was thermally sintered to achieve conducting feedlines. In a second step, the feedlines were passivated using a polyimide-based ink. Two MEA layouts were designed and printed. The first layout was printed on a temperature-stable polyimide foil and contained 28 electrodes for cell recordings. The second layout was printed on a polyethylene-naphtalate substrate and contained 64 microelectrodes. The microelectrodes had a diameter of about 31 µm and were separated by a pitch of 200 µm. Impedance measurements were conducted to characterize the interfacial capacitance of the microelectrodes. Extracellular measurements from HL-1 cells grown on the microelectrode arrays demonstrated the feasibility of using printed MEAs for recording action potentials. In total, peak-to-peak amplitudes of about 36 µV at a signal-to-noise ratio of ~17 were observed. The cellular origin of the recorded signals was demonstrated by chemically stimulating the cells with noradrenaline, which lead to an increased frequency in the recorded signals. Overall, this work demonstrates that inkjet printing can be applied to easily fabricate disposable sensing devices for cell-based bioelectronic applications. Although the inkjet technology inherently limits the resolution of the structures, we believe that this approach can be used in the future to provide low-cost disposable alternatives to microfabricated electrode array devices.

5. Acknowledgements

We gratefully acknowledge funding from the Helmholtz Young Investigators Program (VH-NG-515), Helmholtz Validation Fund (HVF-0034 “LiveCheck”) and the Bernstein Center of Computational Neuroscience (grant number 01GQ1004A, BMBF). Furthermore, we would like to thank Elke Brauweiler-Reuters (FZ Jülich) for performing the SEM imaging, Norbert Wolters (FZ Jülich) for help in designing and building the amplifier system, and Dieter Lomparski (FZ Jülich) for programming the LabView control and visualization software for the amplifier.

6. References

[1] Mack C M, Lin B J, Turner J D, Johnstone A F M, Burgoon L D and Shafer T J 2014 Burst and principal components analyses of {MEA} data for 16 chemicals describe at least three effects classes *NeuroToxicology* **40** 75 – 85

[2] Johnstone A F M, Gross G W, Weiss D G, Schroeder O H-U, Gramowski A and Shafer T J 2010 Microelectrode arrays: A physiologically based neurotoxicity testing platform for the 21st century *NeuroToxicology* **31** 331 – 350

[3] Hondebrink L, Verboven A H A, Drega W S, Schmeink S, Groot M W G D M de, Kleef R G D M van, Wijnolts F M J, Groot A de, Meulenbelt J and Westerink R H S 2016 Neurotoxicity screening of (illicit) drugs using novel methods for analysis of microelectrode array (MEA) recordings *NeuroToxicology* **55** 1 – 9

[4] Yeung C K, Sommerhage F, Wrobel G, Offenhäusser A, Chan M and Ingebrandt S 2007 Drug profiling using planar microelectrode arrays *Anal. Bioanal. Chem.* **387** 2673–2680

[5] Latifi S, Tamayol A, Habibey R, Sabzevari R, Kahn C, Geny D, Eftekharpour E, Annabi N, Blau A, Linder M and Arab-Tehrany E 2016 Natural lecithin promotes neural network complexity and activity *Sci. Rep.* **6** 25777

[6] Yakushenko A, Kätelhön E and Wolfrum B 2013 Parallel On-Chip Analysis of Single Vesicle Neurotransmitter Release *Anal. Chem.* **85** 5483–5490

[7] Wang J, Trouillon R, Lin Y, Svensson M I and Ewing A G 2013 Individually Addressable Thin-Film Ultramicroelectrode Array for Spatial Measurements of Single Vesicle Release *Anal. Chem.* **85** 5600–5608

[8] Berdondini L, Imfeld K, Maccione A, Tedesco M, Neukom S, Koudelka-Hep M and Martinoia S 2009 Active pixel sensor array for high spatio-temporal resolution electrophysiological recordings from single cell to large scale neuronal networks *Lab. Chip* **9** 2644–2651

[9] Müller J, Ballini M, Livi P, Chen Y, Radivojevic M, Shadmani A, Viswam V, Jones I L, Fiscella M, Diggelmann R, Stettler A, Frey U, Bakkum D J and Hierlemann A 2015 High-resolution CMOS MEA platform to study neurons at subcellular, cellular, and network levels *Lab. Chip* **15** 2767–2780

[10] Allitt B J, Harris A R, Morgan S J, Clark G M and Paolini A G 2016 Thin-film micro-electrode stimulation of the cochlea in rats exposed to aminoglycoside induced hearing loss *Hear. Res.* **331** 13 – 26

[11] Bai Q and Wise K D 2001 Single-unit neural recording with active microelectrode arrays *IEEE Trans. Biomed. Eng.* **48** 911–920

[12] Czeschik A, Rinklin P, Derra U, Ullmann S, Holik P, Steltenkamp S, Offenhausser A and Wolfrum B 2015 Nanostructured cavity devices for extracellular stimulation of HL-1 cells *Nanoscale* **7** 9275–9281

[13] Kang X, Liu J, Tian H, Yang B, NuLi Y and Yang C 2016 Sputtered iridium oxide modified flexible parylene microelectrodes array for electrical recording and stimulation of muscles *Sens. Actuators B Chem.* **225** 267 – 278

[14] Krause K J, Yakushenko A and Wolfrum B 2015 Stochastic On-Chip Detection of Subpicomolar Concentrations of Silver Nanoparticles *Anal. Chem.* **87** 7321–7325

[15] Brüggemann D, Wolfrum B, Maybeck V, Mourzina Y, Jansen M and Offenhäusser A 2011 Nanostructured gold microelectrodes for extracellular recording from electrogenic cells *Nanotechnology* **22** 265104

[16] Xie C, Lin Z, Hanson L, Cui Y and Cui B 2012 Intracellular recording of action potentials by nanopillar electroporation *Nat. Nano* **7** 185–190

[17] Hofmann B, Kätelhön E, Schottdorf M, Offenhäusser A and Wolfrum B 2011 Nanocavity electrode array for recording from electrogenic cells *Lab. Chip* **11** 1054–1058

[18] Santoro F, Dasgupta S, Schnitker J, Auth T, Neumann E, Panaitov G, Gompper G and Offenhäusser A 2014 Interfacing Electrogenic Cells with 3D Nanoelectrodes: Position, Shape, and Size Matter *ACS Nano* **8** 6713–6723

[19] Heim M, Yvert B and Kuhn A 2012 Nanostructuration strategies to enhance microelectrode array (MEA) performance for neuronal recording and stimulation *Neuronal Ensemble Rec. Integr. Neurosci.* **106** 137–145
[20] VanDersarl J J and Renaud P 2016 Biomimetic surface patterning for long-term transmembrane access *Sci. Rep.* **6** 32485
[21] Adams C, Mathieson K, Gunning D, Cunningham W, Rahman M, Morrison J D and Prydderch M L 2005 Development of flexible arrays for in vivo neuronal recording and stimulation *Nucl. Instrum. Methods Phys. Res. Sect. Accel. Spectrometers Detect. Assoc. Equip.* **546** 154 – 159
[22] Blau A, Murr A, Wolff S, Sernagor E, Medini P, Iurilli G, Ziegler C and Benfenati F 2011 Flexible, all-polymer microelectrode arrays for the capture of cardiac and neuronal signals *Biomaterials* **32** 1778 – 1786
[23] David-Pur M, Bareket-Keren L, Beit-Yaakov G, Raz-Prag D and Hanein Y 2014 All-carbon-nanotube flexible multi-electrode array for neuronal recording and stimulation *Biomed. Microdevices* **16** 43–53
[24] Lacour S P, Benmerah S, Tarte E, FitzGerald J, Serra J, McMahon S, Fawcett J, Graudejus O, Yu Z and Morrison B 2010 Flexible and stretchable micro-electrodes for in vitro and in vivo neural interfaces *Med. Biol. Eng. Comput.* **48** 945–954
[25] Larmagnac A, Eggenberger S, Janossy H and Vörös J 2014 Stretchable electronics based on Ag-PDMS composites *Sci. Rep.* **4** 7254
[26] Blaschke B M, Lottner M, Drieschner S, Bonaccini Calia A, Stoiber K, Rousseau L, Lissourges G and Garrido J A 2016 Flexible graphene transistors for recording cell action potentials *2D Mater.* **3** 025007
[27] Khodagholy D, Gelinas J N, Thesen T, Doyle W, Devinsky O, Malliaras G G and Buzsaki G 2015 NeuroGrid: recording action potentials from the surface of the brain *Nat. Neurosci* **18** 310–315
[28] Liu J, Fu T-M, Cheng Z, Hong G, Zhou T, Jin L, Duvvuri M, Jiang Z, Kruskal P, Xie C, Suo Z, Fang Y and Lieber C M 2015 Syringe-injectable electronics *Nat. Nano* **10** 629–636
[29] Wolfrum B, Kätelhön E, Yakushenko A, Krause K J, Adly N, Hüske M and Rinklin P 2016 Nanoscale Electrochemical Sensor Arrays: Redox Cycling Amplification in Dual-Electrode Systems *Acc. Chem. Res.* **49** 2031–2040
[30] Gans B-J de, Duineveld P C and Schubert U S 2004 Inkjet Printing of Polymers: State of the Art and Future Developments *Adv. Mater.* **16** 203–213
[31] Shimoni A, Azoubel S and Magdassi S 2014 Inkjet printing of flexible high-performance carbon nanotube transparent conductive films by “coffee ring effect” *Nanoscale* **6** 11084–11089
[32] Speakman S P, Rozenberg G G, Clay K J, Milne W I, Ille A, Gardner I A, Bresler E and Steinke J H G 2001 High performance organic semiconducting thin films: Ink jet printed polythiophene [rr-P3HT] *Org. Electron.* **2** 65 – 73
[33] Hamad E M, Bilatto S E R, Adly N Y, Correa D S, Wolfrum B, Schöning M J, Offenhäusser A and Yakushenko A 2016 Inkjet printing of UV-curable adhesive and dielectric inks for microfluidic devices *Lab. Chip* **16** 70–74
[34] Delaney J T, Smith P J and Schubert U S 2009 Inkjet printing of proteins *Soft Matter* **5** 4866–4877
[35] Roth E A, Xu T, Das M, Gregory C, Hickman J J and Boland T 2004 Inkjet printing for high-throughput cell patterning *Biomaterials* **25** 3707 – 3715
[36] El-Molla S, Albrecht A, Cagatay E, Mittendorfer P, Cheng G, Lugli P, Salmerón J F and Rivadeneyra A 2016 Integration of a Thin Film PDMS-Based Capacitive Sensor for Tactile Sensing in an Electronic Skin *J. Sens.* **2016** 7
[37] Wu J, Wang R, Yu H, Li G, Xu K, Tien N C, Roberts R C and Li D 2015 Inkjet-printed microelectrodes on PDMS as biosensors for functionalized microfluidic systems *Lab Chip* **15** 690–695
[38] Setti L, Fraleoni-Morgera A, Ballarin B, Filippini A, Frascaro D and Piana C 2005 An amperometric glucose biosensor prototype fabricated by thermal inkjet printing *Biosens. Bioelectron.* **20** 2019–2026
[39] Li J, Rossignol F and Macdonald J 2015 Inkjet printing for biosensor fabrication: combining chemistry and technology for advanced manufacturing *Lab. Chip* **15** 2538–2558

[40] Vuorinen T, Niittynen J, Kankkunen T, Kraft T M and Mäntysalo M 2016 Inkjet-Printed Graphene/PEDOT:PSS Temperature Sensors on a Skin-Conformable Polyurethane Substrate *Sci. Rep.* **6** 35289
[41] Chow E, Herrmann J, Barton C S, Raguse B and Wieczorek L 2009 Inkjet-printed gold nanoparticle chemiresistors: Influence of film morphology and ionic strength on the detection of organics dissolved in aqueous solution *Anal. Chim. Acta* **632** 135–142
[42] Hu C, Bai X, Wang Y, Jin W, Zhang X and Hu S 2012 Inkjet Printing of Nanoporous Gold Electrode Arrays on Cellulose Membranes for High-Sensitive Paper-Like Electrochemical Oxygen Sensors Using Ionic Liquid Electrolytes *Anal. Chem.* **84** 3745–3750
[43] Kim Y, Kim J W, Kim J and Noh M 2017 A novel fabrication method of Parylene-based microelectrodes utilizing inkjet printing *Sens. Actuators B Chem.* **238** 862–870
[44] Lesch A, Momotenko D, Cortés-Salazar F, Wirth I, Tefashe U M, Meiners F, Vaske B, Girault H H and Wittstock G 2012 Fabrication of soft gold microelectrode arrays as probes for scanning electrochemical microscopy *J. Electroanal. Chem.* **666** 52–61
[45] Xu Z, Dong Q, Otieno B, Liu Y, Williams I, Cai D, Li Y, Lei Y and Li B 2016 Real-time in situ sensing of multiple water quality related parameters using micro-electrode array (MEA) fabricated by inkjet-printing technology (IPT) *Sens. Actuators B Chem.* **237** 1108–1119
[46] Jensen G C, Krause C E, Sotzing G A and Rusling J F 2011 Inkjet-printed gold nanoparticle electrochemical arrays on plastic. Application to immunodetection of a cancer biomarker protein *Phys. Chem. Chem. Phys. PCCP* **13** 4888–4894
[47] Roberts T, De Graaf J B, Nicol C, Hervé T, Fiocchi M and Sanaur S 2016 Flexible Inkjet-Printed Multielectrode Arrays for Neuromuscular Cartography *Adv. Healthc. Mater.* **5** 1462–1470
[48] Khan Y, Pavinatto F J, Lin M C, Liao A, Swisher S L, Mann K, Subramanian V, Maharbiz M M and Arias A C 2016 Bioelectronic Interfaces: Inkjet-Printed Flexible Gold Electrode Arrays for Bioelectronic Interfaces *Adv. Funct. Mater.* **26** 981–981
[49] Swisher S L, Lin M C, Liao A, Leeflang E J, Khan Y, Pavinatto F J, Mann K, Naujokas A, Young D, Roy S, Harrison M R, Arias A C, Subramanian V and Maharbiz M M 2015 Impedance sensing device enables early detection of pressure ulcers in vivo *Nat. Commun.* **6** 6575
[50] Bard A J and Faulkner L R 2001 *Electrochemical Methods: Fundamentals and Applications* (New York: Wiley)
[51] Claycomb W C, Lanson N A, Stallworth B S, Egeland D B, Delcarpio J B, Bahinski A and Izzo N J 1998 HL-1 cells: A cardiac muscle cell line that contracts and retains phenotypic characteristics of the adult cardiomyocyte *Proc. Natl. Acad. Sci. U. S. A.* **95** 2979–2984
[52] Deegan R D, Bakajin O, Dupont T F, Huber G, Nagel S R and Witten T A 1997 Capillary flow as the cause of ring stains from dried liquid drops *Nature* **389** 827–829
[53] Soltman D and Subramanian V 2008 Inkjet-Printed Line Morphologies and Temperature Control of the Coffee Ring Effect *Langmuir* **24** 2224–2231
[54] Buffat P and Borel J-P 1976 Size effect on the melting temperature of gold particles *Phys Rev A* **13** 2287–2298
[55] Cui W, Lu W, Zhang Y, Lin G, Wei T and Jiang L 2010 Gold nanoparticle ink suitable for electric-conductive pattern fabrication using in ink-jet printing technology *Colloids Surf. Physicochem. Eng. Asp.* **358** 35–41
[56] Määttänen A, Ihalainen P, Pulkkinen P, Wang S, Tenhu H and Peltonen J 2012 Inkjet-Printed Gold Electrodes on Paper: Characterization and Functionalization *ACS Appl. Mater. Interfaces* **4** 955–964
[57] Bakhishev T and Subramanian V 2009 Investigation of Gold Nanoparticle Inks for Low-Temperature Lead-Free Packaging Technology *J. Electron. Mater.* **38**
[58] Huang D, Liao F, Molesa S, Redinger D and Subramanian V 2003 Plastic-Compatible Low Resistance Printable Gold Nanoparticle Conductors for Flexible Electronics *J. Electrochem. Soc.* **150** G412–G417
[59] Cortie M B, Maaroof A I and Smith G B 2005 Electrochemical capacitance of mesoporous gold *Gold Bull.* **38** 14–22

[60] Rutten W L C 2002 Selective Electrical Interfaces with the Nervous System *Annu. Rev. Biomed. Eng.* **4** 407–452
[61] Rocha P R F, Schlett P, Kintzel U, Mailänder V, Vandamme L K J, Zeck G, Gomes H L, Biscarini F and Leeuw D M de 2016 Electrochemical noise and impedance of Au electrode/electrolyte interfaces enabling extracellular detection of glioma cell populations *Sci. Rep.* **6** 34843